Conductance spectroscopy in coupled quantum dots

Gerhard Klimeck,* Guanlong Chen,† and Supriyo Datta
School of Electrical Engineering, Purdue University, West Lafayette, Indiana 47907-1285
(Received 14 December 1993; revised manuscript received 28 March 1994)

We investigate the linear-response conductance through a pair of coupled quantum dots. The conductance spectrum under ideal conditions is shown to consist of two sets of twin peaks whose locations and amplitudes are determined by the interdot coupling and the intradot charging. We will show that the qualitative features of the spectrum survive against experimental nonidealities such as (1) detuning of the individual dots, (2) interdot charging, (3) inelastic scattering, and (4) multiple lateral states. The effect of higher lateral states depends strongly on the nature of the interaction potential, screening lengths, and exchange terms, but the lowest set of twin peaks is largely unaffected by these details.

I. INTRODUCTION

Single quantum dots have been widely studied and a clear understanding of the transport through these artificial atoms has emerged.[1] Coupled quantum dots could be considered as artificial molecules and their study could open up new physics in which electron charging and electron coherence play a significant role. Most studies of coupled quantum dots include *only* charging.[2–7] Few studies[8,9] have been performed on coupled quantum dots in which coherence and charge quantization are considered simultaneously.

The purpose of this paper is to calculate the conductance spectrum including coherence and charging interactions. Our approach is very similar to that developed by Beenakker[10] and Meir et *al.*[11] for single dots. The main difference is that we calculate the exact many-body states of the "molecule" rather than a single "atom." We start with the ideal case of (1) identical dots, (2) no interdot charging, and (3) a single spin-degenerate lateral state in each dot. We then examine some effects of nonidealities that are inevitable in an experiment. Due to numerical limitations, our method can be applied to a maximum of 12 single-particle states, which is not sufficient to describe present day lateral structures. However, improved lithographic techniques will eventually allow lateral structures with fewer electrons. Using present day technology vertical structures can be fabricated having very few electrons.[12–15] Such structures typically do not have a gate electrode[16,17] which is necessary for linear-response measurements. However, using shadow evaporation a sidewall gate could be fabricated as shown in Fig. 1.

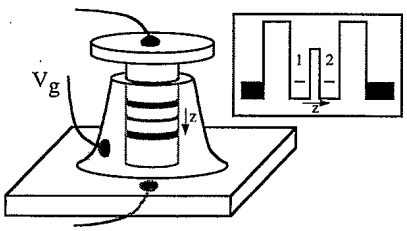

FIG. 1. Proposed experimental setup for a sidewall-gated small-cross-section vertical triple barrier structure. Inset shows the simplified conduction band in the central region in the growth direction. Fermi energy and lateral confinement can be changed with the gate voltage V_g.

A system of two coupled quantum dots with one doubly spin-degenerate single-particle state in each dot (2×2 single-particle states) will exhibit four conductance peaks.[18,19] These peaks coincide with the fluctuation of the equilibrium number of electrons in the quantum dot as transitions 0→1, 1→2, 2→3, and 3→4 occur. These transitions of electron numbers in the quantum dot are expected to occur at characteristic Fermi energies that are determined by the transition energies of the many-body states in the quantum dot. The coupling strength t between the quantum dots and the charging interaction energy U in a single quantum dot determine the separation between the four conductance peaks. Here we show that the expected double set of twin peaks in the conductance determined by the characteristic energies t and U survives against experimental nonidealities such as (1) detuning of the bare energy levels of the quantum dots due to variations in confinement, (2) interdot interactions, (3) multiple lateral states with off-diagonal interactions, and (4) inelastic scattering.

II. MODEL

We consider a system described by a Hamiltonian with four terms: the coupled quantum dot (H_D), the charge interaction in the coupled quantum dot (H_C), the leads (H_L), and the coupling of the leads to the quantum dot (H_T).

$$H = H_D + H_C + H_L + H_T\,, \tag{1a}$$

$$H_D = \sum_{\alpha;m;i} \epsilon_{im\alpha} c^\dagger_{im\alpha} c_{im\alpha} + \sum_{\alpha;m} \left(t_m c^\dagger_{1m\alpha} c_{2m\alpha} + \text{c.c.} \right) , \tag{1b}$$

$$H_C = \sum_{i;m,n,p,q,\alpha,\beta} U_{i;m,n,p,q} c^\dagger_{i;m,\alpha} c^\dagger_{i;n,\beta} c_{i;p,\beta} c_{i;q,\alpha} + \sum_{\alpha,\beta;m,n} W_{m,n} n_{1m\alpha} n_{2n\beta} , \tag{1c}$$

$$H_L = \sum_{\alpha;m;k\in L,R} \epsilon_{km\alpha} c^\dagger_{km\alpha} c_{km\alpha} , \tag{1d}$$

$$H_T = \sum_{\alpha;m;k\in L} \left(V^L_{km\alpha} c^\dagger_{1m\alpha} c_{km\alpha} + \text{c.c.} \right) + \sum_{\alpha;m;k\in R} \left(V^R_{km\alpha} c^\dagger_{2m\alpha} c_{km\alpha} + \text{c.c.} \right) . \tag{1e}$$

The variables k and i symbolize states in the leads and the ith quantum dot, respectively. α and β are spin indices, and m,n,p,q are lateral quantum numbers. $U_{i;m,n,p,q}$ represents the intradot, lateral-state-dependent repulsion in dot i. The interdot charge interaction and interdot coupling between the two quantum dots are represented by $W_{m,n}$ and t_m, respectively. The tunneling matrix element V^L_{km} (V^R_{km}) connects dot 1 (2) to the left (right) lead. We assume the lateral confinement to be homogeneous and do not consider effects due to subband mixing[20] and energy dependence of coupling.

We assume the coupled quantum dots to be *weakly* coupled to the leads, such that H_T can be treated to first order in perturbation for single-particle transitions. We evaluate the Hamiltonians H_D and H_C describing the decoupled "molecule" in the subset of constant numbers of electrons via direct diagonalization[21,23] in the basis of Slater determinants. We treat the coupled quantum dot as a *single* coherent system and use a conductance formula[10,11] which was developed for single quantum dots. However, the transition rates are more complicated in our case, since the spatial structure of the interacting eigenstates is more complicated:

$$G = \frac{e^2}{k_B T} \sum_{n=1}^{N_{\max}} \sum_{ij} \frac{\Gamma^L_{nij} \Gamma^R_{nij}}{\Gamma^L_{nij} + \Gamma^R_{nij}} P^{\text{eq}}_{n,i} \times [1 - f(E_{n,i} - E_{n-1,j} - \mu)] , \tag{2}$$

where Γ^L_{nij} indicate transitions from the ith n-particle state to the jth $(n-1)$-particle state via transitions through the left barrier. $P^{\text{eq}}_{n,i}$ indicates the equilibrium occupation of the initial state (n,i) with eigenenergy $E_{n,i}$ calculated with

$$P^{\text{eq}}_{n,i} = \frac{1}{Z} \exp\left[-\frac{1}{k_B T} (E_{n,i} - n\mu) \right] , \tag{3a}$$

$$Z = \sum_{n,i} \exp\left[-\frac{1}{k_B T} (E_{n,i} - n\mu) \right] , \tag{3b}$$

where μ is the chemical potential in the leads. The electronic states in the leads are assumed to be one-dimensional (1D) subbands filled according to Fermi-Dirac statistics and $(1-f)$ indicates the probability to find an empty state in the lead, which satisfies the energy conservation requirement for the $(n,i) \rightarrow (n-1,j)$ transition. We assume the temperature to be high enough such that we can neglect the Kondo effect due to correlations of electrons in the leads with electrons in the central system.

III. RESULTS

A. Ideal case

We start with the ideal case of a system consisting only of a single lateral, doubly spin-degenerate state in each quantum dot. The conduction band we assume for our analysis is depicted in the inset of Fig. 1. We assume the interdot charging to be zero (W=0) and assume the single-particle ground states in the two dots to be aligned with each other (ϵ_1=ϵ_2=ϵ). The one-particle ground state of the coupled system is the bonding state with eigenenergy E_1=ϵ−t. Throughout this work we consider the case where the charging energy U is larger than the interdot coupling t. Consequently, electrons tend to distribute themselves throughout the structure to avoid the on-site charging energy and the two-particle ground state has an eigenenergy of E_2=2ϵ+$O(t^2)$. The third electron has to "pay" charging energy in one of the quantum dots and the ground state of the three-particle ground state is $E_3 = 3\epsilon + U - t$. The fourth electron fills up the given orbitals and the eigenenergy of the four-particle many-body ground state is E_4=4ϵ+2U. Single-particle transitions which alter the number of electrons in the quantum dot can therefore occur at four particular Fermi energies: $\epsilon - t$, $\epsilon + t$, $\epsilon + U - t$, and $\epsilon + U + t$.

We have calculated the conductance spectrum for energy-independent tunneling matrix elements $V^{L/R}_{k\alpha}$ with a single-particle single-barrier transition rate Γ=1 μeV assuming that ϵ=30 meV, t=1 meV, and U=5 meV. The resulting conductance G (solid line) is depicted in Fig. 2 with the corresponding average number of electrons in the quantum dot $\langle N \rangle$ (dashed line), as a function of Fermi energy. Note that the conductance peaks occur whenever the number of particles changes. There

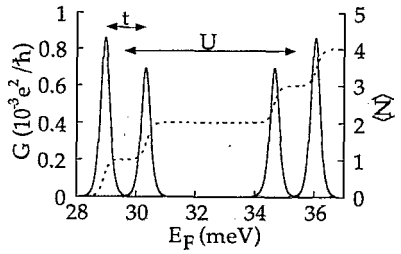

FIG. 2. Conductance G (solid line) calculated for a system of coupled, symmetric quantum dots as a function of Fermi energy E_F. Conductance peaks are grouped by charging energy U and coupling energy t. Transitions in the total number of electrons N (dashed line) in the quantum dot coincide with the conductance peaks.

are four conductance peaks corresponding to the filling of the quantum dot system with four electrons. We obtain two sets of twin peaks where the "twins" are separated by the interdot coupling energy t and the sets are separated by the intradot repulsion U. The upper two peaks are the energetic mirror image of the lower two taken at midgap, which is due to electron-hole symmetry in the problem. Note that the second peak is smaller than the first peak *not* due to any energy dependence of the tunneling rate, but due to the spatial and energetic structure of the many-body states in the dot.[18]

B. Detuning

Nonuniformities in the lateral or the longitudinal confinement of the quantum dots will lead to some detuning Δ of the single-electronic ground states between the two dots (inset in Fig. 3). Figure 3 compares the calculated conductance for the coupled quantum dot system we discussed above for three different detunings (a) $\Delta=0$, (b) $\Delta=U$, and (c) $\Delta=2U$. The conductance G is plotted on the same linear scale in all three plots. Note that the first and fourth peak decrease in amplitude while the second and third peak are roughly unchanged in (a) and (b). Not only do the amplitudes of the four peaks change, but also their locations, indicative of changes in the excitation spectrum of the coupled quantum dots.

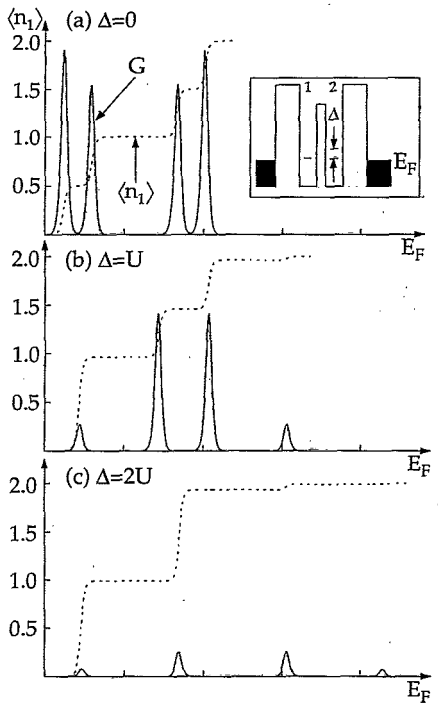

FIG. 3. Conductance spectra G (solid line) for different degrees of detuning Δ of the second quantum dot against the first quantum dot (inset). (a)–(c) show G on the same scale for Δ=0, Δ=U, and Δ=2U in arbitrary units. Dashed line shows the average number of electrons in the first quantum dot ($\langle n_1 \rangle$).

Figure 4 analyzes the conductance peak spectrum (a) and amplitudes (b) separately as a function of detuning Δ. The amplitudes of peaks 1 and 4 (dashed lines) are equal as well as the amplitudes of peaks 2 and 3 (solid line). As the single-particle eigenenergy of the decoupled dots is raised in the second quantum dot, the first electron tends to localize in the first dot of the coupled system and the localization increases with detuning. The eigenenergy of the composite single-particle ground state changes [Fig. 4(a)] from $E_1=\epsilon-t=29$ meV ($\Delta=0$) to $E_1=\epsilon=30$ meV ($\Delta=\infty$). As a result of the decreasing probability of finding the electron in the right well, the amplitude of the first conductance peak [Fig. 4(b)] decreases rapidly with detuning ($\propto \frac{t^2}{\Delta^2}$). For a symmetric structure without detuning we have equal probability to find an electron in the left or the right quantum dot [$\langle n_1 \rangle=0.5$ in Fig. 3(a)]. Figure 3(b) shows the average number of electrons in quantum dot 1 ($\langle n_1 \rangle$) at a detuning of Δ=5 meV as a function of the Fermi energy. The average of $\lesssim 1$ past the first conductance peak indicates the localization of the first electron in quantum dot 1.

Formally we denote the many-body states in an occupation number notation of the form $|n_{1\uparrow}, n_{1\downarrow}, n_{2\uparrow}, n_{2\downarrow}\rangle$, where the index 1 (2) refers to the left (right) dot and $\uparrow, \downarrow$ are spin indices. Using this notation we find that the one-particle ground state is twofold degenerate with one up-spin and one down-spin state. We denote them (neglecting the normalization) as $|\psi_{1\uparrow}\rangle = |1,0,0,0\rangle - \alpha|0,0,1,0\rangle$ and $|\psi_{1\downarrow}\rangle = |0,1,0,0\rangle - \alpha|0,0,0,1\rangle$, where $\alpha \propto \frac{t}{\Delta}$. The probability to find an electron in dot 2 and the coupling to the right lead by transitions into state $|0,0,0,0\rangle$ is

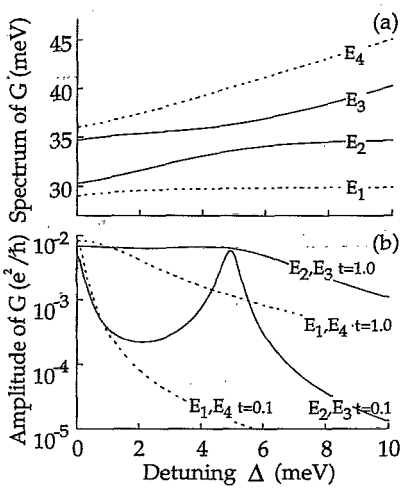

FIG. 4. (a) Conductance peak spectrum as a function of detuning. Δ=0 shows two sets of twin peaks at 29,30 and 35,36 meV for ϵ_0=30 meV, U=5 meV, and t=1 meV. Anticrossing is visible at $\Delta=U=5$ meV. (b) Amplitudes of conductance peaks as a function of detuning. Dashed lines correspond to the first and fourth peaks in (a). Solid lines correspond to the second and third peaks in (a). Interdot coupling t is a parameter. Second and third peaks are almost independent of detuning Δ if t is large enough.

proportional to α^2.

Intuitively one expects the second conductance peak to exhibit the same behavior with detuning as the first peak. Given small detuning, $\Delta \ll U$, the two-particle ground state is given[23] by $|\psi_2\rangle \approx |1,0,0,1\rangle + |0,1,1,0\rangle$ (neglecting normalization). Transitions through the left barrier (e.g., $\langle\psi_{1\uparrow}|c_{1\downarrow}|\psi_2\rangle \approx \alpha$, where $c_{1\uparrow}$ is the up-spin destruction operator in dot 1) are limited by the localization of an electron in dot 1 and the weak leakage to dot 2. This is one possible current contribution to the second conductance peak. The intradot charge interaction introduces a resonance feature (at $\Delta = U$) that allows for a second transport process through the quantum dot at even higher detuning. The argument is as follows. When $\Delta = U$ we have a degeneracy of the three[23] basis states $|1,0,0,1\rangle$, $|0,1,1,0\rangle$, and $|1,1,0,0\rangle$, which make up the ground state. The basis state $|1,1,0,0\rangle$ can couple well with the one-particle ground states $|\psi_{1\uparrow}\rangle \approx |1,0,0,0\rangle$ and $|\psi_{1\downarrow}\rangle \approx |0,1,0,0\rangle$ via transitions through the *left* barrier. The basis states $|1,0,0,1\rangle$ and $|0,1,1,0\rangle$ are well coupled to $|\psi_{1\uparrow}\rangle$ and $|\psi_{1\downarrow}\rangle$ by transitions through the *right* barrier. The two-particle ground state is therefore well coupled to the one-particle ground state via transitions through the *left* and the *right* barrier and the second conductance peak is large. Figure 3(b) indicates an average number of electrons in the first quantum dot of $\lesssim 1.5$ in the case of equal detuning and intradot charging. $\Delta = U$ is the transition region where the "energetic payment" to reside in a higher single-particle level in dot 2 or the charging energy against the first electron in dot 1 are equal. This means that the second electron is actually 50% of the time in the first quantum dot "next" to the localized first electron.

Increased detuning where $\Delta > U$ will tend to localize *both* electrons in quantum dot 1 and the ground state will consist mostly of basis state $|1,1,0,0\rangle$. Figure 3(c) indicates an average number of electrons of $\lesssim 2$ out of two electrons total in quantum dot 1 past the second conductance peak. The conductance will then decrease rapidly with Δ since no electrons are in quantum dot 2 to be coupled to the right, similar to the behavior of the first peak amplitude.

The region of intermediate detuning where the detuning is smaller than the intradot charging energy ($0 < \Delta < U$) is determined by a "competition" between the two transport processes discussed above. The first process is dependent on the leakage $\alpha \propto \frac{t}{\Delta}$ of the one-particle state into dot 2. The second process is dependent on the mixing of the $|1,1,0,0\rangle$ basis state into the two-particle ground state. The two-particle ground state is a spin 0 state and can be denoted as[23] $|\psi_2\rangle = |1,0,0,1\rangle + |0,1,1,0\rangle + \beta|1,1,0,0\rangle$, neglecting normalization, where $\beta \propto \frac{t}{U-\Delta}$ for $\Delta \ll U$. Transition contributions due to $\alpha \propto \frac{t}{\Delta}$ (localization of the first electron) decrease with detuning and contributions due to $\beta = \frac{t}{U-\Delta}$ (mixing of $|1,1,0,0\rangle$) increase with detuning. Both contributions are proportional to the interdot coupling t, and the amplitude of the second conductance peak appears to be almost independent of detuning if the strength of the interdot coupling is strong enough [Fig. 4(b)].

The third and fourth conductance peaks can be most easily understood by the formal electron-hole symmetry in our notation. Every "electron" Slater determinant (e.g., $|1,0,0,0\rangle$) has a complementary "hole" Slater determinant (e.g., $|0,1,1,1\rangle$). The same arguments that we have given for the first two conductance peaks in terms of electron localization can be extended to arguments following hole localization. We can explain the first conductance peak with the transition of the first electron into the system from the $|0,0,0,0\rangle$ state; similarly, we can explain the fourth conductance peak with the transition of the first hole into the system from the $|1,1,1,1\rangle$ state. Conductance peaks 1 and 4 have therefore the same amplitude as functions of Δ (see Fig. 4). Indeed, we find the amplitudes of peaks 2 and 3 to be the same functions of Δ.

It is interesting to note that the conductance peaks coincide with fluctuations in the total number of particles in the quantum dot. Given the discrete energy spectrum of this system, the total number of particles always increases by 1 (see Fig. 2) with the same slope at every step (assuming small temperatures) independent of the detuning of the quantum dots ($\frac{\partial\langle N\rangle}{\partial\mu}$ is the same for all transitions.). The conductance amplitude, however, is dependent on the spatial structure of the composite many-body eigenstates and depends on the detuning.

Figure 4(a) shows the spectrum of the excitation energies of the coupled quantum dot as a function of detuning. An anticrossing of the second and third excitation is visible at a detuning of $\Delta = U$ where the localization of one electron changes to the localization of two electrons in one quantum dot. We can see [Fig. 4(b)] how conductance peak 1 (4) decreases rapidly with Δ due to localization of the first electron (last hole) and peak 2 (3) decreases after localization of two electrons (holes). Although the relative amplitude and the spectrum of the conductance peaks change with detuning we still expect the double set of twin peaks to be observable. It is important to design the experimental structure such that the coupling between the two quantum dots is strong enough to compensate for detunings, which are inevitable due to inhomogeneities in the confinement.

C. Interdot charging

Another physical process that may distort the double set of twin peaks in the conductance spectrum is interdot charging. With significant charge interaction[8] it seems reasonable that a strongly localized wave function in one quantum dot causes a non-negligible potential in the neighboring quantum dot. Figure 5 shows the conductance peak spectrum (a) and amplitude (b) calculated as a function of interdot charging for the ideal structure discussed above. We have scanned the value of interdot charging from 0 meV up to the value of intradot charging of U=5 meV. Neither the locus nor the amplitude of the first conductance peak change, since the addition and extraction of the first electron into and out of the system does not involve any interdot charging energy.

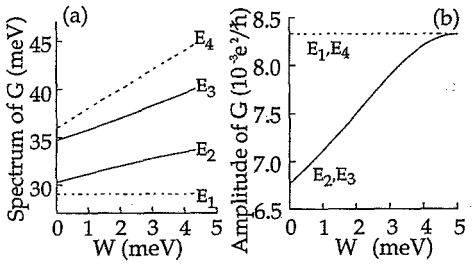

FIG. 5. (a) Conductance peak spectrum as a function of interdot charging W. First peak is unchanged, fourth peak changes linearly with interdot charging. (b) Amplitudes of conductance peaks. Dashed line corresponds to peaks 1 and 4 in (a). Peaks 2 and 3 (solid line) increase until all four peaks have the same amplitude at $W=U$ where interdot and intradot charging energies are the same.

The locus of the second conductance peak becomes separated (almost) linearly from the first conductance peak as the interdot charging is increased linearly since the eigenenergies of the dominant[23] Slater determinants $|1,0,0,1\rangle$ and $|0,1,1,0\rangle$ are $2\epsilon+W$. The two Slater determinants $|1,1,0,0\rangle$ and $|0,0,1,1\rangle$ have eigenenergies of $2\epsilon+U$. The strength of their mixture into the two-particle ground state increases with the decrease in U–W. Since $|1,1,0,0\rangle$ and $|0,0,1,1\rangle$ are the states that allow for transport through the structure, as discussed above for the state $|1,1,0,0\rangle$, we expect the conductance to increase with an increased mixture of these basis states into the ground state.

The spatial separation of charges into different quantum dots ($|1,0,0,1\rangle$,$|0,1,1,0\rangle$) is energetically not preferable anymore once the limit of $W=U$ is reached. Indeed the degeneracies of the coupled dot eigenstate develop such that the first and the second conductance peaks have the same amplitude in this limit. The loci of the third and fourth conductance peaks separate themselves from the previous peak with the same proportionality to interdot charging. The amplitude of the third and fourth conductance peaks can be explained in the same fashion as for the first and second peaks by electron-hole symmetry.[24]

Notice that the double set of twin peaks is preserved even when interdot charging is included in the model. However, note that the separation of the conductance peaks does contain some information about the interdot charging energy. The energy difference between the first two and the last two peaks cannot be identified with the interdot coupling t. Similarly, the separation between the two sets of peaks cannot be identified with the intradot charging energy U.

D. Multiple lateral states with off-diagonal interactions

We now consider the influence of multiple lateral states on the conductance spectrum of the coupled quantum dots. The lateral confinement determines the single-particle energy quantization in the lateral dimensions. Strong confinements resulting in level separations of ΔE=30–50 meV have been observed.[12,25] These values are larger than the observed[14,15] single-electron charging energies which are of the order of 0.5–5 meV. If the lateral energy quantization ΔE is comparable[26,27,15] to the charging energies U and the coupling t, we expect the excited lateral states to be mixed into the ground states of the coupled system. This would destroy the appearance of a double set of twin peaks in the conductance spectrum discussed above. The basic questions we try to answer in this section are the following. (1) How strong does the confinement have to be, such that the double set of twin peaks is not destroyed by the mixing in of higher lateral states? (2) Does the off-diagonal character of the exchange terms in the Hamiltonian have any influence on the symmetry of the twin peaks which are induced by the off-diagonal interdot coupling?

Calculations of the many-body states of single[28–33] and coupled[34] quantum dots have been performed. They mostly differ by their choice of interaction potential, $V(\vec{r}_1-\vec{r}_2)$, and the number of particles included in the system. Since we are interested in the N-particle ground states given relatively strong confinement we restrict ourselves to the lowest lateral single-particle modes in the system and include as many particles as these states can hold. In order to estimate single-particle eigenenergies and charging energies we consider a model system of a single rectangular quantum dot with hard walls[35] and vary the lateral width of the quantum dot ($d_x = d_y$). We consider the three lowest single-particle eigenstates described by their lateral quantum number (n_x, n_y): $(1,1)\rightarrow 1$, $(2,1)\rightarrow 2$, and $(1,2)\rightarrow 3$, and number them 1, 2, 3. We assume the longitudinal or transport dimension to be much smaller than the lateral confinement ($d_z = 50$ Å) and consider only the ground state in that dimension ($n_z = 1$). Using this simple model we calculate the interaction energies

$$U_{mnpq} = \iint d\vec{r}_1 d\vec{r}_2\, V(\vec{r}_1-\vec{r}_2)\ \phi_m^*(\vec{r}_1) \times\phi_n^*(\vec{r}_2)\ \phi_p(\vec{r}_2)\ \phi_p(\vec{r}_1)\ , \qquad (4)$$

which appear in the Hamiltonian.

By symmetry in the given limited set of basis states one can show that all other interaction energies but U_{mnmn}, U_{mmnn}, and U_{mnnm} are zero. In particular we are left with the direct integrals $V_{11}=U_{1111}$, $V_{22}=U_{2222}$, $V_{12d}=U_{1221}=U_{2112}=U_{1331}=U_{2112}$, and $V_{23d}=U_{2332}=U_{3223}$, and the exchange integrals $V_{12e}=U_{1212}=U_{2121}=U_{1122}=U_{2211}=U_{1313}=U_{3131}=U_{1133}=U_{3311}$ and $V_{23e}=U_{2323}=U_{3232}=U_{2233}=U_{3322}$. We have used three different interaction potentials, the unscreened[28,29] Coulomb potential $\frac{e^2}{4\pi\epsilon}\frac{1}{|\vec{r}_1-\vec{r}_2|}$, the saturated[32,36] Coulomb potential $\frac{e^2}{4\pi\epsilon}\frac{1}{\sqrt{|\vec{r}_1-\vec{r}_2|^2+\alpha^2}}$, and the screened Coulomb potential $\frac{e^2}{4\pi\epsilon}\frac{\exp(-|\vec{r}_1-\vec{r}_2|/\beta)}{|\vec{r}_1-\vec{r}_2|}$ for comparison. Figure 6(a) depicts the four direct charging energies, the two exchange energies, and the single-particle excitation energy $\Delta E=E_2-E_1=E_3-E_1$ for the unscreened Coulomb potential. As a relative measure we also depicted the single-particle excitation energy of the next lowest lateral single-

particle state, $\Delta E_{\rm negl} = E_{n_x=2,n_y=2} - E_1$, which has been neglected in our calculation here. The single-particle excitation energies show the well known $1/d_x^2$ dependence, whereas the charging energies in Fig. 6(a) show a weaker dependence on the lateral dimension. As long as the single-particle excitation energy $\Delta E = E_2 - E_1$ is significantly larger than the charging energies we expect the mixing of the higher lateral states into the ground state of the two-particle ground state for the single quantum dot to be weak. For a coupled dot system we would therefore expect the double set of twin peaks to survive certainly for $d_x < 300$ Å [Fig. 6(a)].

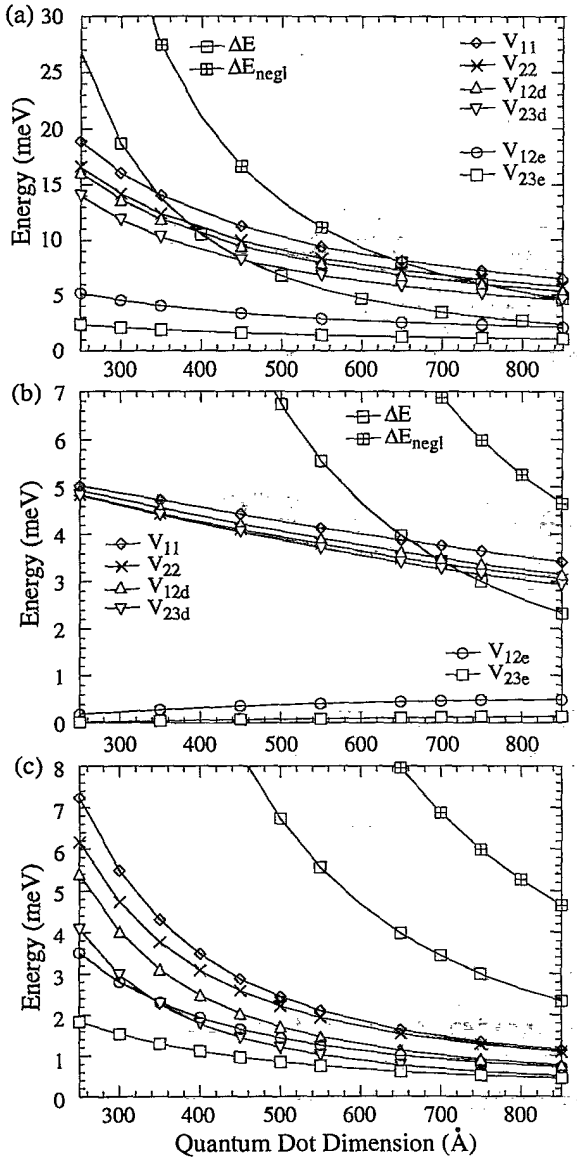

FIG. 6. Direct (V_{11}, V_{22}, V_{12d}, V_{23d}) and exchange (V_{12e}, V_{23e}) Coulomb integrals and single-particle excitation energies $\Delta E = E_2 - E_1$ and $\Delta E_{\rm negl}$ as a function of lateral confinement $d_x = d_y$ for (a) unscreened Coulomb potential, (b) saturated Coulomb potential ($\alpha = 200$ Å), and (c) screened Coulomb potential ($\beta = 50$ Å).

The charging energies for small quantum dots depicted in Fig. 6(a) are of the order of 15 meV, which are larger than the charging energies that have been observed[14,15] so far in single quantum dots (0.5–5 meV). A screening length of $\alpha = 200$ Å in the saturated Coulomb potential reduces the charging energies down to the experimental level of about 5 meV as depicted in Fig. 6(b), where the length of 200 Å corresponds to the average distance away from the large carrier densities in the emitter and collector which could be considered as ground planes. Given these reduced charging energies we expect that the quantum dot can be much wider now without mixing of the higher lateral states into the 1–4-particle ground states. The region of "allowed" quantum dot size is extended to at least $d_x = 600$ Å in this simple model. Notice that the exchange energies are significantly smaller than the direct energies for this choice of potential.

Using the exponentially screened potential with β=50 Å we obtain the charging energies depicted in Fig. 6(c). Notice that the exchange terms are comparable to the direct terms and become identical to their corresponding direct term for large cross sections. This indicates that the charging energies between electrons of the same spin in different orbitals are negligible for large cross sections.

In view of the differences in the interaction energies for different models for the Coulomb interaction, we would expect the conductance spectra to be different too. Figures 7(a) and 7(b) show the conductance spectra for

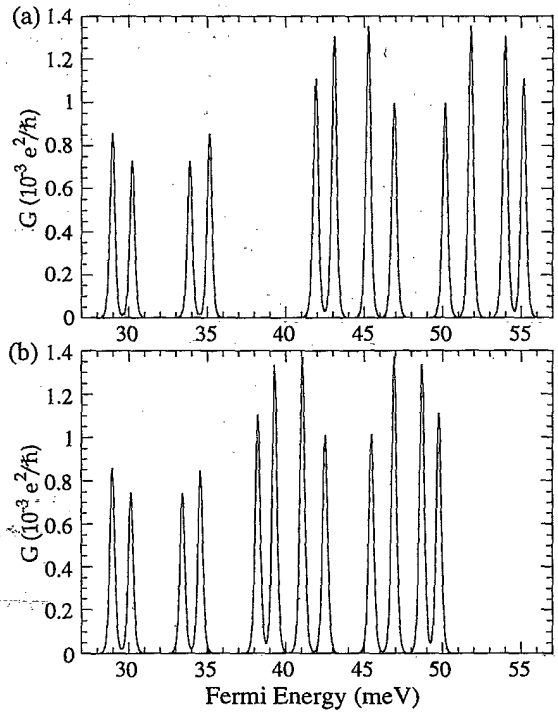

FIG. 7. Conductance spectrum calculated with $\epsilon_0 = 30$ meV, $t = 1$ meV, $k_B T = 0.1$ meV, and the interaction energies calculated with the saturated Coulomb potential [Fig. 6(b)] for two different quantum dot sizes (a) $d_x = d_y = 550$ Å and (b) $d_x = d_y = 750$ Å.

$d_x = d_y = 550$ Å and for $d_x = d_y = 750$ Å corresponding to the saturated Coulomb potential [Fig. 6(b)]. The lowest set of twin peaks is clearly decoupled from the upper peaks arising from the higher lateral modes even for a quantum dot dimension as large as 750 Å. But when we use the screened Coulomb potential [Fig. 6(c)] we find that, although the decoupling is quite clear at $d_x = d_y = 550$ Å, it is not as clear for $d_x = d_y = 750$ Å [Figs. 8(a) and 8(b)]. We also find that if we set the exchange terms in the interaction to zero, the higher peaks are affected but the lowest set of twin peaks is left unchanged.

Figures 9(a) and 9(b) show the conductance spectra calculated using the unscreened Coulomb potential. In this case, too, the lowest set of twin peaks is clearly resolved at low temperatures ($k_BT \ll t$). But at higher temperatures, the symmetry of this set of twin peaks is significantly affected for the large quantum dot ($d_x = d_y = 750$ Å). We attribute this to the mixing of the lateral states 2 and 3 into the three- and four-particle states close to the the ground state. The temperature dependence is nontrivial and reflects the occupation of excited states in the coupled dot system, which all have quite different couplings to the leads. It is interesting to note that the fifth and sixth peaks for the $d_x = d_y = 750$ Å case are extremely weak. We find that if we set the exchange energies to zero in our calculation these two peaks become comparable to peaks 7–12. As we have already noted above, the inclusion of the exchange term does affect the upper part of the spectrum though it has little effect on the lowest set of twin peaks.

Given the uncertainty in the actual nature of the screening and confinement potentials, our main conclusion in this section is that we expect the double set of twin peaks to survive against the mixing in of higher lateral states for quantum dot dimensions up to ≈ 750 Å.[35] Screening of the Coulomb interaction leads to lower interaction energies and therefore increases the size of the quantum dot for which we expect higher lateral states not to affect the lower set of twin peaks. The exchange terms in the interaction affect the upper part of the conductance spectra but have no effect on the lowest set of twin peaks.

E. Inelastic scattering

We can account for strong inelastic scattering by using the following expression for G instead of Eq. (2):

$$G_{\text{in}} = \frac{e^2}{k_BT} \sum_{n=1}^{N_{\max}} P_n^{\text{eq}} \frac{\langle\langle \Gamma_n^L \rangle\rangle \langle\langle \Gamma_n^R \rangle\rangle}{\langle\langle \Gamma_n^L \rangle\rangle + \langle\langle \Gamma_n^R \rangle\rangle}, \tag{5}$$

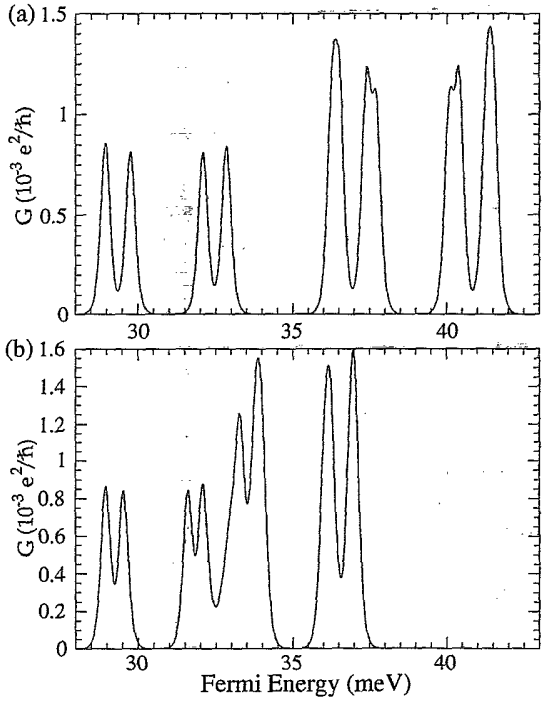

FIG. 8. Conductance spectrum calculated with $\epsilon_0 = 30$ meV, $t = 1$ meV, $k_BT = 0.1$ meV, and the interaction energies calculated with the screened Coulomb potential [Fig. 6(c)] for two different quantum dot sizes (a) $d_x = d_y = 550$ Å and (b) $d_x = d_y = 750$ Å.

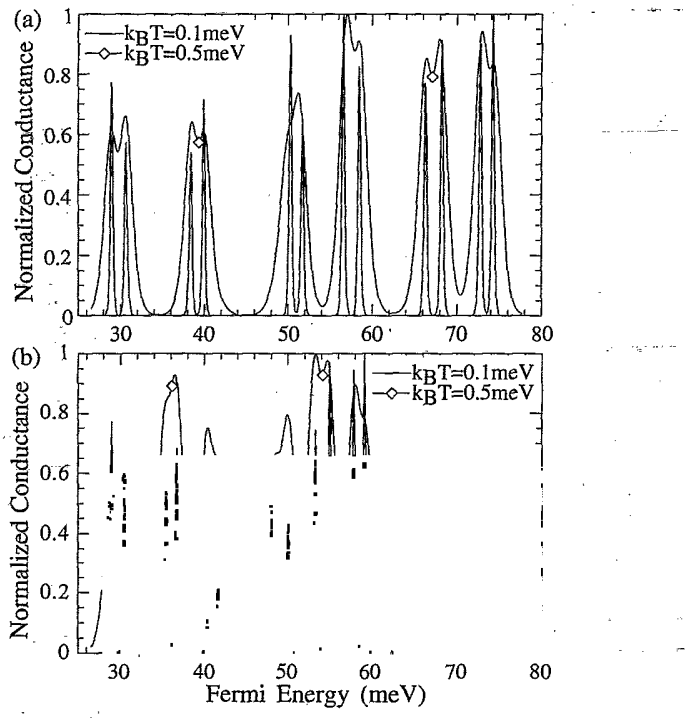

FIG. 9. Conductance spectrum calculated with $\epsilon_0 = 30$ meV, $t = 1$ meV, and the interaction energies calculated with the pure Coulomb potential [Fig. 6(a)] for two different quantum dot sizes (a) $d_x = d_y = 550$ Å. The double set of twin peaks is well separated from peaks 5–12 and symmetry between the two sets persists for high temperatures. (b) $d_x = d_y = 750$ Å. Conductance still shows a double set of "twin" peaks at low temperature but the high temperature calculations show the broken symmetry of peaks 1 and 4 and peaks 2 and 3 due to mixing in of higher lateral states.

where

$$\langle\langle \Gamma_n^{L(R)} \rangle\rangle = \sum_{ij} \Gamma_{nij}^{L(R)} F_{\rm eq}(E_{n,i}|n) \times [1 - f(E_{n,i} - E_{n-1,j} - \mu)] , \quad (6a)$$

$$P_n^{\rm eq} = \sum_i P_{n,i}^{\rm eq} , \quad (6b)$$

$$F_{\rm eq}(E_{n,i}|n) = \frac{1}{Z_n} \exp\left(-\frac{E_{n,i}}{k_B T}\right) , \quad (6c)$$

$$Z_n = \sum_i \exp\left(-\frac{E_{n,i}}{k_B T}\right) . \quad (6d)$$

This formula is essentially the same as that derived by Beenakker[10] for single quantum dots. The main difference is that the coupling terms $\Gamma^{L(R)}$ have been modified to account for the nature of the electronic states in coupled quantum dots. The effect of inelastic scattering in linear response is to thermally average all transitions through the left and the right barrier [Eq. (6a)] for the subset of constant number of electrons, n, in the quantum dot. $F_{\rm eq}(E_{n,i}|n)$ is the canonical distribution function indicating the conditional probability of state (n,i) being occupied, given n electrons in the system.

The two conductance formulas in Eqs. (2) and (5) give the same[10] result under two independent conditions if (1) $\Gamma_{nij}^L/\Gamma_{nij}^R = \text{const}, \forall(nij)$, or (2) $k_B T \ll E_{n,\text{excited}} - E_{n,\text{ground}}$. For the nonidealities we have considered in this paper condition (1) is only violated in the case of detuning. Detuning introduces an asymmetry into the eigenstates of the system such that the ratio of left lead to right lead coupling becomes state dependent. We find that the amplitudes of the conductance peaks do change due to inclusion of inelastic scattering; however, the general shape of the conductance peaks does not change in the case of $k_B T \approx t$. The features due to interdot coupling t will be thermally broadened and cannot be resolved in this limit. Since we are interested in resolving features of energy scale t, we require temperatures with $k_B T \ll t$ and Eqs. (2) and (5) will give the same results [condition (2) from above].

IV. CONCLUSIONS

We have presented calculations of conductance spectra for two strongly coupled quantum dots that are weakly coupled to the adjoining leads. The conductance spectrum due to the first four electrons consists of a double set of twin peaks. The location of the conductance peaks coincides with transitions in the total number of electrons in the quantum dot. However, the peak amplitude is strongly dependent on the spatial properties of the many-body states in the quantum dots and varies from one peak to another although $\frac{\partial\langle N\rangle}{\partial\mu}$ is the same for every transition. We analyze the effect of experimental nonidealities such as quantum dot detuning, interdot charging, multiple lateral states with off-diagonal interactions, and inelastic scattering on the conductance spectrum. We find that the spectrum is altered due to the first three effects, but the qualitative features persist. We suggest that in an experiment the interdot coupling be made sufficiently strong such that detuning due to variations in confinement does not decrease the amplitudes of the conductance peaks significantly. We find that interdot charging as well as inelastic scattering have little effect on the spectrum. We show that for quantum dot dimensions[35] $\lesssim 750$ Å higher lateral states do not change the symmetry of the lower conductance peaks, which consists of a double set of twin peaks as expected for the ideal structure. This lower part of the spectrum is unaffected by the choice of interaction potentials, exchange terms, etc., although the upper part of the spectrum (due to higher lateral modes) is strongly influenced by these details.

ACKNOWLEDGMENTS

One of us (G.C.) acknowledges fruitful discussions in the early stages of this work with Dr. Guanhua Chen, in which the double-peak picture emerged. Helpful discussions and critical reviews by M. P. Anantram and discussion with Chris Bowen are greatly appreciated by G.K. This work has been supported by the National Science Foundation (Grants No. ECS-9201446 and No. ECS-9110980).

* Present address: Eric Jonsson School of Engineering and Computer Science, University of Texas at Dallas, Richardson, TX 75083-0688 .
† Present address: Department of Electrical and Computer Engineering and Beckmann Institute, University of Illinois, Urbana, IL 61801.

[1] M. A. Kastner, Rev. Mod. Phys. **64**, 849 (1992).
[2] L. I. Glazman and V. Chandrasekhar, Europhys. Lett. **19**, 623 (1992).
[3] A. A. Middleton and N. S. Wingreen (unpublished).
[4] P. Delsing, in *One-Dimensional Arrays of Small Tunnel Junctions*, edited by H. Grabert and M. H. Devoret (Plenum, New York, 1992), Chap. 7, pp. 249–273.
[5] L. P. Kouwenhoven *et al.*, Phys. Rev. Lett. **65**, 361 (1990).
[6] M. Tewordt *et al.*, Appl. Phys. Lett. **60**, 595 (1992).
[7] R. J. Haug, J. Hong, and K. Lee, Surf. Sci. **263**, 415 (1992).
[8] G. W. Bryant, Phys. Rev. B **44**, 3064 (1991).
[9] C. Fong *et al.*, Phys. Rev. B **46**, 9538 (1992).
[10] C. W. J. Beenakker, Phys. Rev. B **44**, 1646 (1991).
[11] Y. Meir, N. S. Wingreen, and P. A. Lee, Phys. Rev. Lett. **66**, 3048 (1991).
[12] M. A. Reed *et al.*, Phys. Rev. Lett. **60**, 535 (1988).
[13] S. Tarucha, Y. Hirayama, T. Saku, and T. Kimura, Phys. Rev. B **41**, 5459 (1990).
[14] M. Tewordt *et al.*, Phys. Rev. B. **45**, 14 407 (1992).
[15] B. Su, J. V. Goldman, and J. E. Cunningham, Phys. Rev. B **46**, 7644 (1992).
[16] M. W. Dellow *et al.*, Electron. Lett. **27**, 134 (1991).
[17] P. Guéret, N. Blanc, R. Germann, and H. Rothuizen, Phys. Rev. Lett. **68**, 1896 (1992).

[18] G. Klimeck, Ph. D. thesis, Purdue University, 1994.
[19] G. Chen, G. Klimeck, and S. Datta (unpublished).
[20] G. Klimeck, S. Datta, R. K. Lake, and G. W. Bryant, Phys. Rev. B (to be published).
[21] E. Dagotto *et al.*, Phys. Rev. Lett. **67**, 1918 (1991).
[22] E. Kaxiras and E. Manousakis, Phys. Rev. B **37**, 656 (1988).
[23] The states $|1,0,1,0\rangle$ and $|0,1,0,1\rangle$ are not included in the two-particle ground state since they are not coupled to any other state in the set of six Slater determinants by the interdot coupling t. They are therefore two degenerate eigenstates of the coupled system with eigenenergy $\epsilon_1+\epsilon_2$. The basis state $|0,0,1,1\rangle$ is left out in this argument here because it has an energy of $2\epsilon+2\Delta+U$ as diagonal entry in the $N=2$ Hamiltonian, which is significantly higher in energy than the diagonal element $2\epsilon+U$ of basis state $|1,1,0,0\rangle$, and its contribution to the ground state is negligible.
[24] References 18 and 22 show how interdot charging breaks the electron-hole symmetry in a finite chain of quantum dots, due to localization of charge at the edges of the chain. The electron-hole symmetry is not broken here because only two equivalent dots are involved.
[25] S. Tarucha, Y. Hirayama, and Y. Tokura, Appl. Phys. Lett. **58**, 1623 (1991).
[26] B. Su, J. V. Goldman, M. Santos, and M. Shayegan, Appl. Phys. Lett. **58**, 747 (1991).
[27] J. V. Goldman, B. Su, and J. E. Cunningham, in *Nanostructures and Mesoscopic Systems*, edited by W. P. Kirk and M. A. Reed (Academic Press, Boston, 1991), pp. 173–182.
[28] G. W. Bryant, Phys. Rev. Lett. **59**, 1140 (1987).
[29] P. A. Maksym and T. Chakraborty, Phys. Rev. Lett. **65**, 108 (1990).
[30] N. F. Johnson and M. C. Payne, Phys. Rev. B **45**, 3819 (1992).
[31] B. L. Johnson and G. Kirczenow, Phys. Rev. B **47**, 10 563 (1993).
[32] W. Häusler and B. Kramer, Phys. Rev. B **47**, 16 353 (1993).
[33] A. Kumar, S. E. Laux, and F. Stern, Phys. Rev. B **42**, 5166 (1990).
[34] G. W. Bryant, Physica B **189**, 34 (1993).
[35] Although hard wall potentials are not completely realistic they serve to give a rough estimate for the wave functions needed to calculate the interaction energies.
[36] N. F. Johnson and M. C. Payne, Superlatt. Microstruct. **11**, 309 (1992).